The Cytoplasmic Domain of proEGF Negatively Regulates Motility and Elastinolytic Activity in Thyroid Carcinoma Cells[1]

Aleksandra Glogowska*, Janette Pyka[†], Astrid Kehlen[‡], Marek Los[§], Paul Perumal*, Ekkehard Weber[¶], Sheue-yann Cheng[#], Cuong Hoang-Vu[†] and Thomas Klonisch*,**

*Department of Human Anatomy and Cell Science, Winnipeg, Manitoba, Canada; [†]Clinics of Surgery, Medical Faculty, Martin Luther University Halle-Wittenberg, Halle, Germany; [‡]Probiodrug AG, Weinbergweg, Halle, Germany; [§]BioAplications Enterprises, Winnipeg, Manitoba, Canada; [¶]Institute of Physiology Chemistry, Medical Faculty, Martin Luther University Halle-Wittenberg, Halle, Germany; [#]Laboratory of Molecular Biology, National Cancer Institute, National Institutes of Health, Bethesda, MD 20892-4264, USA; **Department of Medical Microbiology and Infectious Diseases, Faculty of Medicine, University of Manitoba, Winnipeg, Canada

Abstract

The intracellular domains of the membrane-anchoring regions of some precursors of epidermal growth factor (EGF) family members have intrinsic biologic activities. We have determined the role of the human proEGF cytoplasmic domain (proEGFcyt) as part of the proEGF transmembrane–anchored region (proEGFctF) in the regulation of motility and elastinolytic invasion in human thyroid cancer cells. We found proEGFctF to act as a negative regulator of motility and elastin matrix penetration and the presence of proEGFcyt or proEGF22.23 resulted in a similar reduction in motility and elastinolytic migration. This activity was counteracted by EGF-induced activation of EGF receptor signaling. Decreased elastinolytic migratory activity in the presence of proEGFctF and proEGFcyt/proEGF22.23 coincided with decreased secretion of elastinolytic procathepsin L. The presence of proEGFctF and proEGFcyt/proEGF22.23 coincided with the specific transcriptional up-regulation of t-SNARE member SNAP25. Treatment with siRNA-SNAP25 resulted in motility and elastin migration being restored to normal levels. Epidermal growth factor treatment down-regulated SNAP25 protein by activating EGF receptor–mediated proteasomal degradation of SNAP25. These data provide first evidence for an important function of the cytoplasmic domain of the human proEGF transmembrane region as a novel suppressor of motility and cathepsin L–mediated elastinolytic invasion in human thyroid carcinoma cells and suggest important clinical implications for EGF-expressing tumors.

Neoplasia (2008) 10, 1120–1130

Introduction

The human membrane–anchored epidermal growth factor (EGF) precursor (proEGF) is the founder and largest member (1207 amino acid [aa]) [1] of the EGF-like growth factor family, which also includes heparin binding–EGF (HB-EGF), transforming growth factor alpha (TGFα), β-cellulin, neuregulins 1 to 4, epiregulin, epigen, cripto, and amphiregulin. With the exception of cripto, EGF-like ligands bind to and activate membrane-bound EGF receptors ErbB1, 3, and 4 and have important roles in growth and differentiation [2].

Enhanced tumor aggressiveness and shorter survival periods are positively correlated with the presence of EGF-like ligands and ErbB receptors [3]. Cellular localization and proteolytic processing of membrane-anchored EGF-like precursors through members of the ADAM family of sheddases is controlled by their membrane-anchoring and cytoplasmic domain [4,5] and display tissue and cell type–specific pattern [6–9].

Increasing evidence suggests important functional roles for the transmembrane region and particularly the cytoplasmic domain of EGF receptor (EGFR) ligands [4,5]. The proTGF alpha cytoplasmic domain (proTGFα-cyt) was first described to interact with a kinase complex [10] and was later confirmed to act as a binding partner for a number of proteins involved in the maturation and intracellular trafficking of membrane proteins. These include syntenin/mda-9/TACIP18 (proTGFα-cyt domain-interacting protein 18) [11], Golgi reassembly stacking protein of 55 kDa [12] and membrane-associated guanylate kinase inverted-3 [13]. Naked2, the mammalian homolog of *Drosophila* Naked Cuticle binds proTGFα-cyt and facilitates basolateral sorting of this precursor in MDCK [14]. ProARcyt was also shown to contain residues important for basolateral sorting information [15–17]. The function of the EGFR ligand cytoplasmic domain is not restricted to the maturation and subcellular targeting of the precursor but may be of clinical relevance. The nuclear localization of the cytoplasmic domain of proHB-EGF (proHB-EGFcyt) is linked to aggressive transitional cell carcinoma [18]. Among the interaction partners of proHB-EGFcyt is the survival-promoting co-chaperone protein Bag-1 which increases HB-EGF secretion [19]. On shedding, proHB-EGFcyt translocates to the nucleus, binds to the inner nuclear membrane [20], and interacts with the cyclin A transcriptional repressor promyelocytic leukemia zinc finger protein and its heterodimerization partner B-cell lymphoma 6 (Bcl6) to induce S-phase entry [21,22]. Moreover, phosphorylation has recently been suggested as a novel way to modulate HB-EGFcyt and TGFα-cyt functions [23]. On binding to its ErbB receptor, neuregulin 1 (NRG1) cytoplasmic domain (proNRG1cyt) is released into the cytosol and its association with LIM-kinase 1 has been implicated in visual-spatial cognition [24,25]. Soluble NRG1cyt is also a nuclear transcriptional suppressor for several regulators of apoptosis [24] and enhances the transcriptional activity of the promoter for postsynaptic density protein 95 (PSD-95) by binding to the zinc-finger transcription factor Eos [26]. Finally, we identified human proEGFcyt as a novel modulator of microtubule dynamics and microtubule-associated protein (MAP) 1 and MAP2 production in human thyroid carcinoma [27].

Here, we describe a unique suppressive role of the proEGFcyt as part of the membrane-anchored region of human proEGF in the motility and invasiveness of thyroid cancer cells which involves the SNAP25-mediated suppression of exocytosis of cathepsin L. These findings may be of relevance in human thyroid cancer and have important implications for other types of proEGF-expressing cancers.

Materials and Methods

Cell Culture

Human thyroid follicular carcinoma cell lines FTC-133 and FTC-236 were propagated in HAM's F12 medium and 10% fetal bovine serum (PAA Laboratories GmbH, Pasching, Austria), and the undifferentiated anaplastic human thyroid carcinoma cell line UTC-8305 was grown in RPMI medium plus 20% fetal bovine serum. Stable transfectants of FTC-133 were described previously [27]. Transient transfections of FTC-236 and UTC-8305 were done with 1 µg of the constructs using Lipofectamine (Life Technologies, Burlington, Canada). Transfection efficiency was assessed by an EGFP construct after 24 hours and calculated to be more than 70% for UTC-8305 and 50% to 60% for FTC-236. Protein lysates were harvested 24 hours after transfection for Western blot.

Mouse Model of Follicular Thyroid Carcinoma

The $TR\beta^{PV/PV}$ mouse model of follicular thyroid carcinoma (FTC) with a dominant-negative thyroid receptor β1 mutant PV has been described previously [28–30]. Independent of their sex, $TR\beta^{PV/PV}$ homozygotes develop metastasizing FTC in more than 80% of animals at 6 months [30]. Thyroid tissues were collected at 2.90, 7.73, and 11.93 months of age, fixed in paraformaldehyde, and paraffin-embedded for immunohistochemistry.

RNA Silencing

ProEGFcyt and -proEGF22.23 transfectants of FTC-133 at 60% confluence were transfected with 50 nM siRNA-SNAP25 (5′GGG-TAACAAATGATGCCCG3′; Ambion, Austin, TX) or a nonsilencing, randomized sequence not matching any known human gene (5′AATT-CTCCGAACGTGTCACGT3′) as a control using Lipofectamine 2000 (Life Technologies). After 48 hours, *SNAP25* gene expression and SNAP25 protein levels were assessed by reverse transcription–polymerase chain reaction (RT-PCR) and Western blot analysis, respectively. For siRNA experiments on filters, 20 nM of each siRNA SNAP 25 and nonsilencing siRNA were transfected using the Effectin kit (Qiagen, Ontario, Canada).

RNA processing and RT-PCR

Total RNA of all transfectants was isolated with Trizol reagent (Life Technologies), and RNA amounts were determined by spectrophotometry. Total RNA (1 µg) was used for first-strand cDNA synthesis using the Superscript reverse transcriptase kit and 500 ng/ml of oligo d(T) primer (both Life Technologies). For RT-PCR, 1 µl cDNA and 25 pM each of specific forward and reverse primers were used for SNAP25A+B, SNAP23, and synaptobrevin/VAMP2 (Table 1). The PCR cycle profile consisted of an initial denaturation at 95°C for 15 minutes followed by 40 cycles of denaturation at 95°C for 1 minute, annealing at 60°C for 1 minute, and elongation at 72° for 2 minutes. A negative control devoid of cDNA template was included. Single-PCR products were separated in a 2% agarose gel in TAE buffer (EMD, San Diego, CA) and visualized by ethidium bromide staining.

ProEGFcyt Antiserum

A polyclonal antiserum against human proEGFcyt was generated by immunizing rabbits with a 15-mer palmitylated peptide, purity of >90%,

Table 1. List of Primers Used for RT-PCR.

Target	Primer	Primer Sequence (5′–3′)
SNAP25A	Forward	GGAAATGCTGTGGCCTTTTCATA
SNAP25B	Forward	TCTCATTGCCCATATCCAGG
SNAP25A/B	Reverse	GAAAATTCTGCGGGCTTTGTGTG
SNAP23	Forward	AGGACATGAGAGAGACAGAGAAG
	Reverse	TCTGTTGGTGTCAGCCTTGTCTG
VAMP2	Forward	ATGTCTGCTACCGCTGCCACG
	Reverse	GTAAACTATGATGATGATGAGGATG

derived from a proEGFcyt peptide region encoded by exon 22 (EMC Microcollections, Tuebingen, Germany). Rabbits were immunized subcutaneously with 100 µg of peptide in 400 µl of phosphate-buffered saline (PBS; Sigma, St. Louis, MO) plus 600 µl of complete Freund's adjuvant and subsequently boosted monthly for seven consecutive months by intramuscular injection of 100 µg of peptide in 400 µl of PBS and 600 µl of incomplete Freund's adjuvant.

GST-proEGFcyt Fusion Protein

ProEGFcyt was PCR amplified [27] and the purified and sequenced amplicon was cloned into the *Eco*RI/*Not*I sites of pGEX-5X-1 (Amersham Biosciences, Piscataway, NJ) and transformed into *Escherichia coli*, strain Rosetta 2 (Novagen, EMD Biosciences, Darmstadt, Germany). Cells grown to mid log phase ($OD_{600 \text{ nm}}$ = 0.5-0.7) were induced with 0.1 mM isopropyl-β-D-thiogalactopyranoside (Novagen, EMD Biosciences, Darmstadt, Germany) for 2 hours at room temperature. Total cell protein was extracted from induced and noninduced cultures. Protein expression was verified by electrophoresis of the total cell protein extracts on a 12% SDS-PAGE gel followed by Coomassie staining of the gel. Frozen pellets obtained by centrifugation of 10-ml aliquots of induced GST-proEGFcyt containing Rosetta 2 cultures were resuspended in 600 µl of BugBuster Protein Extraction Reagent (Novagen) supplemented with 12 µl of lysozyme solution of 10 mg/ml (Sigma), 12 U of DNAase (Qiagen), and 2 µl of protease inhibitor cocktail (Sigma) and were incubated for 10 to 15 minutes at room temperature with gentle shaking. The suspension was then centrifuged for 5 minutes at 17,900*g*. The GST-proEGFcyt fusion protein was purified from the clear supernatant using the MicroSpin GST Purification Module (Amersham Biosciences, Piscataway, NJ) according to the manufacturer's instructions. The protein was eluted twice, each by incubating the column for 5 to 10 minutes with 100 µl of glutathione elution buffer. Pooled eluates were run on a 12% SDS-PAGE gel and tested for GST-EGFcyt by Western blot using an anti-GST antiserum (Amersham Biosciences, Piscataway, NJ).

Western Blot Analysis and Inhibition Assay

Transfectants (8.5×10^4 cells per six-well plate) were seeded for 24 hours in serum-free medium plus/minus treatment with EGF (10 ng/ml; Life Technologies), EGFR inhibitor AG1478 (10 µg/ml; Sigma), and MG132 or lactacystine (both 10 µM; Sigma). For Western blot, a monoclonal antibody (mAb) directed against β-actin (1:20,000; Sigma) was used to assess equal loading of proteins. Secreted proteins were recovered from supernatants by centrifuging at 10,000*g* for 15 minutes at 4°C; these were then frozen at –80°C, lyophilized, and resuspended in 1/20th of the original volume with distilled water. Bradford assay (Biorad, Montreal, Canada) was used to determine protein concentrations of supernatants. Equal amounts of supernatant proteins (2 mg/ml) were separated by SDS-PAGE and blotted onto Hybond nitrocellulose membranes (Amersham, Braunschweig, Germany). Nonspecific binding was saturated at room temperature for 1 hour in blocking buffer containing PBS/0.01% Tween 20 (PBST) plus 3% skimmed milk.

For the detection of cath-L forms, membranes were incubated overnight at 4°C with a mAbs specific for procath-L (2D4 at 1:500) and a mAb recognizing all three cath-L forms (33/1 at 1:500) [31], respectively. Other mAbs used were against human SNAP25 (1:400; Cedarlane, Pickering, Ontario, Canada) and anti–EGFR-Tyr 992

(1:1000; Cell Signaling Technology). Human syntaxin1A was detected using a rabbit polyclonal antiserum (1:500; Cedarlane).

Characterization of the polyclonal antiserum against human proEGFcyt (1:1500) was performed with protein extracts of FTC-133-proEGFcyt and mock-stable transfectants (each at 1×10^6 cells per milliliter) under similar conditions as described above. Anti-Xpress antiserum (1:2000; Invitrogen, Carlsbad, CA) was used to detect the Xpress–tagged recombinant proEGFcyt present in FTC-133-proEGFcyt transfectants to confirm the specificity of the new anti-proEGFcyt serum.

A rabbit polyclonal antiserum against human EGF (Z-12; Santa Cruz Biotechnology, Santa Cruz, CA) was used at 1:200 to confirm the presence of EGFctF in stable transfectants. All antibodies were diluted in blocking buffer and membranes were incubated overnight at 4°C. After incubation with a horseradish peroxidase-conjugated goat antimouse Ig (Dianova, Hamburg, Germany; 1:20,000) or a horseradish peroxidase–conjugated goat antirabbit Ig (New England Biolabs, Pickering, Ontario, Canada; 1:4000) for 2 hours at room temperature, specific immunoreactive bands were detected with an ECL-kit (Amersham, Braunschweig, Germany).

For inhibition assays, the polyclonal antiserum against proEGF cyt (1:1000) was incubated with the GST-proEGFcyt fusion protein (8 µg/ml) in 5% powder milk blocking buffer for 4 hours at 4°C before Western blot analyses. Rabbit nonimmune serum was used as a control.

Cell Motility and Elastin Migration Assays

Motility and migration assays were performed on transwell polyethylene membrane filters of 8-µm pore size (Greiner Bio-one, Frickenhausen, Germany) under serum-free conditions as described previously [32]. For 24- (FTC-133) and 48-hour (FTC-133, FTC-236, and UTC-8305) migration assays, 1×10^4 and 1×10^3 cells, respectively, were plated onto filters that had been coated with 40 µl of elastin (50 µg/ml; Sigma). For some experiments, cells were treated for 24 hours with EGF (10 ng/ml), specific EGFR inhibitor AG1478 (10 µg/ml), cath-L inhibitor Z-FF-FMK (5 µM) or the H$^+$–ATPase inhibitor bafilomicin A1 (0.025 µM; all Sigma). Untreated cells and transfectants treated with DMSO solvent (Sigma) at concentrations similar to those used in the inhibitor studies were used as negative controls. Migrated cells were counted in five separate filter areas at 20-fold magnification by bright field microscopy. Mean numbers of migrated cells per filter were determined and presented in the graphs. Results represent three independent experiments with each clone being tested three times with at least three filter sets per experiment.

Incubation with Proteasomal Inhibitors

ProEGFcyt transfectants (8.5×10^4 cells per six-well plate) were incubated for 24 hours in serum-free medium. Cells were pretreated with EGF (10 ng/ml; Life Technologies) for 1, 4, 6, and 24 hours and then treated for 2 hours with proteasome inhibitor MG132 or lactacystine (both 10 µM; Sigma). Cellular proteins were lysed with 1× SDS gel loading buffer before Western blot analysis.

Transmission Electron Microscopy

ProEGFcyt stable transfectants (8.5×10^4 per six-well plate) were incubated for 24 hours before fixation for 1 hour at room temperature in 4% paraformaldehyde, 2.5% glutaraldehyde (both from EMD, Gibbstown, NJ), 8% sucrose in 0.1 M PBS (pH 7.3; both from

Sigma). Cells were rinsed in PBS three times and incubated for 1 hour at room temperature in 1% osmium tetroxide (Sigma) in PBS. Cells were washed five times in double distilled H_2O and dehydrated in a 50% to 100% ethanol series. Sections were covered in 100% of Araldite and incubated overnight at 45°C; images were collected with a CM-10 transmission electron microscope (Philips, Netherlands).

Immunofluorescence and Immunohistochemistry

Immunofluorescent detection of mannose-6-phosphate receptors (M6PR; clone 2G11; 1:200; Abcam, Cambridge, MA; nonacidic endosomes), CD63/LAMP3 (clone NKJ/C3; 1:50; Novocastra, Norwell, MA; lysosomes), and human procath-L (2D4, 1:100) was performed as described previously [32]. An Alexa-Fluor-FITC–conjugated secondary antimurine antibody was used as secondary antibody (1:400; Molecular Probes, Invitrogen). Human *trans*-Golgi network (TGN) and SNAP25 were detected using mAbs against Golgin-97 (1:200, clone CDF4; Molecular Probes) and SNAP25 (1:400, clone CB 59-4B11; Cedarlane). Transfectants were plated onto glass slides and cultured to 80% confluence before fixing in 4% paraformaldehyde in PBS. Blocking of nonspecific binding sites with 10% normal goat serum in PBS plus 2% BSA and 0.05% saponin was done for 30 minutes at room temperature before incubation with primary Ab dilutions in blocking buffer overnight at 4°C. Sections were washed 3 × 10 minutes in PBS and incubated with fluorochrome-conjugated secondary antibody (1:400) for 1 hour at room temperature. Nuclear staining was performed with 0.01 mg/ml Hoechst stain (Sigma). Cells were mounted in fluoroguard antifade reagent (Biorad) and viewed with the Axioplan fluorescent microscope (Zeiss, Jena, Germany); images were captured and processed with an AxioCam camera and Axiovision software (Zeiss), respectively.

For immunohistochemical analysis, 5-μm sections of paraformaldehyde-fixed and paraffin-embedded FTC mouse thyroid tissues were treated with 3% hydrogen peroxidase to block endogenous peroxidase activity. Nonspecific binding were blocked with 3% BSA and 10% goat normal serum (Sigma). After blocking, the sections were incubated with ProEGFcyt antiserum in concentration 1:100 overnight at 4°C. Sections were washed 3 × 10 minutes in PBST buffer and incubated with secondary antibody goat antirabbit (New England Biolabs) for 1 hour at room temperature in a concentration of 1:300. Staining was developed using DAB kit (Pierce, Rockford, IL).

Statistics

All experiments were repeated at least three times. For the stable transfectants, three different clones for each construct were used in all experiments. For migration assays, the mean value with SE and independent 2-tailed *t* test was performed, with $P < .05$ being considered significant. For multiple-experiment comparison, ANOVA table and Tukey's test were used with $P < .05$ being regarded significant.

Results

ProEGFcyt Domain Inhibits Motility of Thyroid Cancer Cells

Stable transfectants of the human FTC cell line FTC-133 containing constructs encoding for previously characterized proEGFcyt constructs [27] and the human EGF, juxtamembrane, transmembrane, and cytoplasmic domain with C-terminal FLAG epitope (EGFctF; gift from Dr. S. Wiley) [4] were used in this study (Figure 1A). ProEGFctF was detected as a single band and membrane-associated protein by Western blot and immunofluorescence using an anti-EGF

and anti-FLAG antibody, respectively (Figure 1, *B* and *C*). Transfectants harboring the empty vector were used as mock control. Transwell filter assays were used to determine the effect of the different proEGFcyt constructs on thyroid tumor cell motility and migration. In the presence of proEGFctF, we observed a 50% reduction in motility compared with mock controls (Figure 1D). Treatment with exogenous EGF enhanced motility, and this increase in motility was mediated by the EGFR as determined by the inability of EGF to increase motility in the presence of the specific EGFR inhibitor AG1478 (Figure 1D) and by the Western blot detection of phosphorylated EGFR Tyr 992 residue on EGF treatment (data not shown). To determine the functional contribution of the proEGF cytoplasmic domain (proEGFcyt), we used the FTC-133 transfectants that exclusively expressed the full cytoplasmic domain of human proEGF (proEGFcyt), an engineered proEGFcyt construct composed of the peptide sequences encoded by exons 22 and 23 of human proEGF (proEGF22.23), and a natural splice form of proEGFcyt lacking the peptide sequences encoded by exons 23 and 24 (proEGFdel23) [27]. Similar to proEGFctF, the presence of proEGFcyt caused a 52% and 41% reduction in cell motility in FTC-133 (Figure 1E) and transiently transfected UTC-8305 (Figure W1A) and FTC-236 thyroid cancer cells (Figure W2A) compared with proEGFdel23 and mock controls, respectively. Soluble EGF significantly increased the motility in transfectants expressing proEGFcyt and proEGF22.23 but not in proEGFdel23 and mock cells. Thus, proEGFcyt, which is part of the transmembrane region encoded by EGFctF, was sufficient to act as a negative regulator of motility in thyroid cancer cells. Moreover, the deletion of exon 23, as in the proEGFdel23, completely abolished the inhibitory effect on thyroid cancer cell motility.

ProEGFcyt Domain Is a Novel Negative Regulator of Elastinolytic Activity

The acquisition of an elastinolytic phenotype by tumor cells is a unique and important requirement for early tissue invasion and facilitates the initial steps of penetration of basal lamina [33,34]. Elastin migration assays revealed a 50% reduction in elastinolytic invasion in the presence of EGFctF (Figure 2A). Similarly, elastin matrix penetration was reduced by 50% and 33% with FTC-133–stable transfectants (Figure 2B) and UTC-8305 (Figure W1B) and FTC-236 (Figure W2B) transient transfectants expressing proEGFcyt and proEGF22.23, respectively, but not with proEGFdel23 and mock transfectants. Exogenous EGF increased the ability of cells to invade elastin matrices, and this effect was most pronounced in the presence of proEGFctF, proEGFcyt, and proEGF22.23 (Figure 2, *A* and *B*). This EGF-induced enhanced elastinolytic migratory activity was dependent on the presence of a functional EGFR and was abolished when the specific EGFR inhibitor AG1478 was used (Figure 2, *A* and *B*). Thus, we identified human proEGFcyt, and here particularly the peptide encoded by exon 23, as the component within the proEGF transmembrane region, which was capable of suppressing the elastin matrix invasion in thyroid cancer cells. Next, we studied the relationship between the tissue expression of proEGFcyt and *in vivo* thyroid carcinogenesis. We hypothesized that proEGFcyt levels will diminish in thyroid tissues at advanced stages of thyroid carcinogenesis. We used our established mouse model of FTC in which FTC mice develop thyroid cancer starting as early as 5 to 6 months [30]. The anti-proEGFcyt rabbit polyclonal serum recognized both human and mouse proEGFcyt as well as recombinant
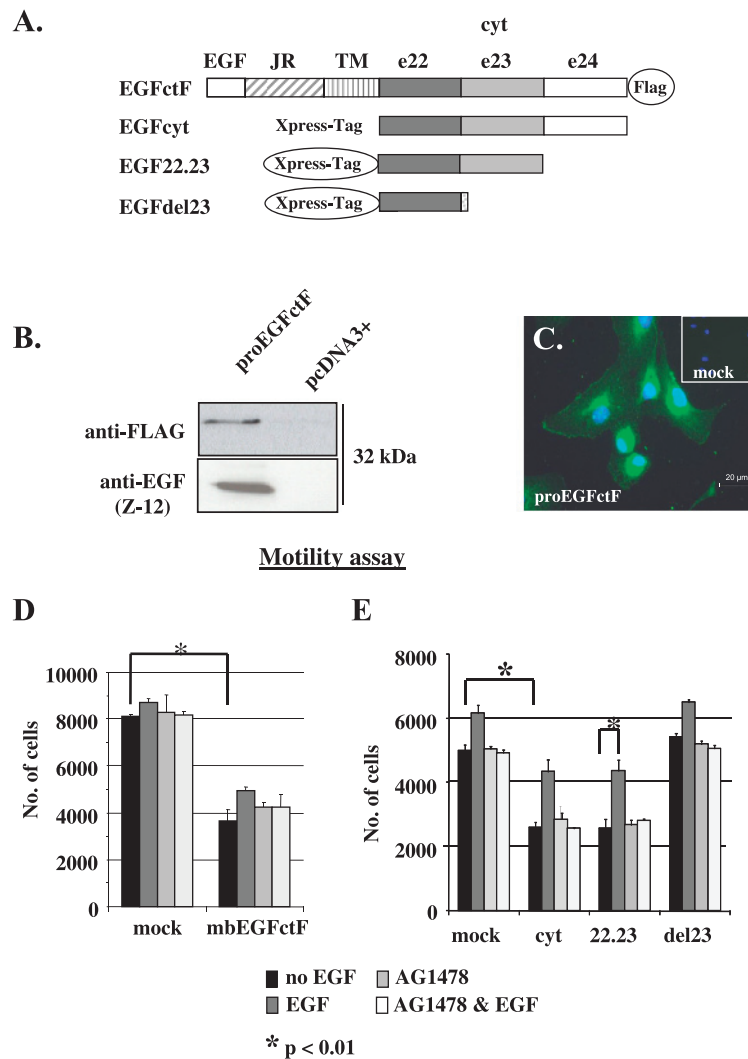
Figure 1. Effect of transmembrane and intracellular motifs of proEGF on cells' motility and elastinolytic migratory activity. (A) Schematic drawing of the different human proEGF constructs used in this study. *cyt* indicates cytoplasmic domain; *e22-24*, exons 22-24; *JR*, juxtamembrane region; *TM*, transmembrane domain. (B) Stable FTC-133–proEGFctF transfectants expressed the characterized transmembrane proEGF construct [4] as detected by antibodies against extracellular EGF and Flag located at the C-terminus of the proEGFctF construct, respectively. (C) Immunofluorescent detection of Flag antigen confirmed the previously reported association of proEGFctF with the plasma membrane and the endosomal/Golgi compartment in FTC-133–proEGFctF stable transfectants. (D) We observed a >50% reduction in cell motility in the presence of proEGFctF and (E) proEGFcyt and proEGF22.23 in FTC-133 transfectants. No change in cell motility was observed with proEGFdel23 or mock transfectants compared with mock controls (E). When exogenous EGF (10 ng/ml) was added, a small increase in motility was observed in the presence of proEGFctF (D). However, an almost complete recovery to mock motility values was observed in proEGFcyt and proEGF22.23 clones (E). Exogenous EGF caused only a slight increase in cell movement with proEGFdel23 and mock transfectants (E). The EGF-induced increase in motility observed with proEGFctF, proEGFcyt and proEGF22.23 stable transfectants was abolished in the presence of the specific EGFR inhibitor AG1478 (10 μg/ml; D and E), indicating the involvement of EGF-activated EGFR signaling pathways. AG1478 alone failed to have any effect on cell motility. Results of three independent motility and migration assay experiments with three filter sets per experiments are shown.

human proEGFcyt in FTC-133–proEGFcyt clones (Figure W3). Immunodetection with this antiserum was blocked with a GST-bound human proEGFcyt fusion protein (Figure 2*C*). Hyperplastic thyroid tissues collected at 2.9 months (Figure 2*F*) showed already a significant decrease in immunoreactive proEGFcyt compared with normal thyroid control tissue (Figure 2*D*). Tumor tissues from 7.73 and 11.93 months were largely devoid of immunoreactive proEGFcyt (Figure 2, *G* and *H*), as was normal thyroid tissue in which the primary antiserum had been replaced with nonimmune rabbit serum (Figure 2*E*). Thus, the down-regulation of proEGF was an early event during mouse thyroid carcinogenesis.

Decreased Elastinolytic Activity Coincides with Diminished procath-L Secretion and an Altered Vesicular Phenotype

The lysosomal hydrolase cath-L has potent elastinolytic activity. We performed Western blot analysis with the well-characterized mAb 33/1, which detects all three human cath-L forms [31]. Total cell lysates (CLs) revealed processed cath-L as proform (43 kDa), single-chain (31 kDa), and processed two-chain cath-L represented by the heavy chain (24 kDa). All FTC-133 clones (Figure 3*A*) and UTC-8305 (Figure W1*C*) and FTC-236 (Figure W2*C*) transient transfectants displayed decreased levels of single-chain cath-L compared with FTC-133–proEGFdel23 and mock controls (Figure 3*A*).
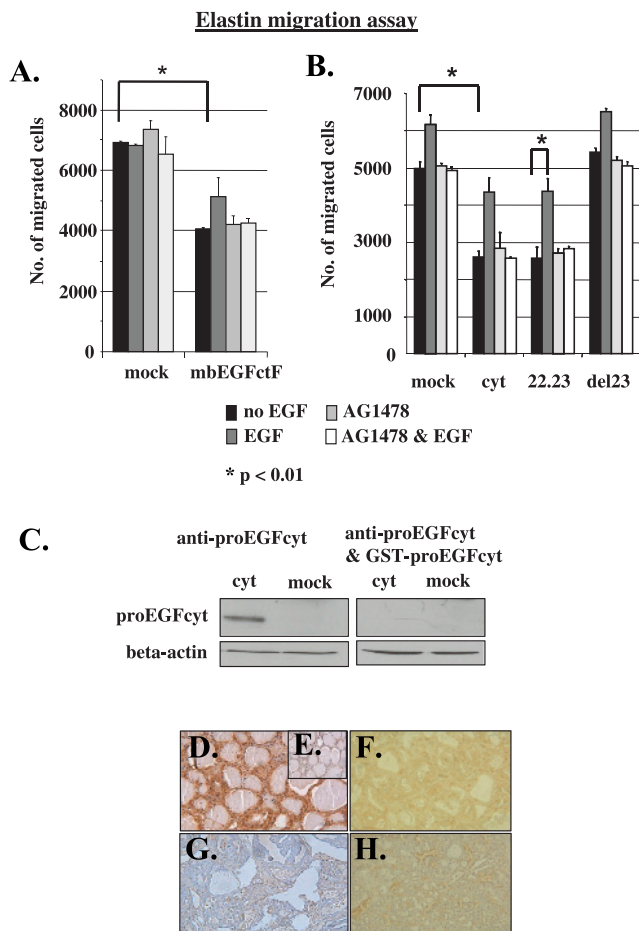
Elastin migration assay

A.

B.

■ no EGF ▨ AG1478
■ EGF □ AG1478 & EGF

* p < 0.01

C.

anti-proEGFcyt   anti-proEGFcyt & GST-proEGFcyt

proEGFcyt

beta-actin

Figure 2. Effect of proEGFcyt signaling on elastinolytic migration activity. Elastin migration assays demonstrated a marked reduction in the ability of human thyroid carcinoma transfectants to penetrate an elastin matrix in the presence of proEGFctF (A) and proEGFcyt and proEGF22.23 compared with proEGFdel23 and mock controls (B). Treatment with exogenous EGF (10 ng/ml) resulted in a significant increase in migration through the elastin matrix, and this was most pronounced with proEGFcyt and proEGF22.23 transfectants (B). The EGF-induced increase in elastinolytic migratory activity was mediated by the EGFR and was abolished in the presence of the specific EGFR inhibitor AG1478 (10 μg/ml). AG1478 itself had no effect (B). Results of three independent motility and migration assay experiments with three filter sets per experiments are shown. For Western blot analysis, we used a newly generated rabbit antiserum against two pooled peptides that were located within the C-terminus of exon 22 of human proEGF cytoplasmic domain (C). This antiserum detected human proEGFcyt in lysates of proEGFcyt stable transfectants, and binding was inhibited in the presence of excess GST-proEGFcyt human recombinant protein (C). The antiserum against proEGFcyt cross-reacted with mouse antigen and detected proEGFcyt in thyroid tissue sections of normal mice (D). Immunostaining was largely abolished in thyroid tissues of FTC mice at 2.90 (F), 7.73 (G), and 11.93 months (H) and was absent in thyroid section where the primary antiserum had been replaced by rabbit nonimmune serum (E).
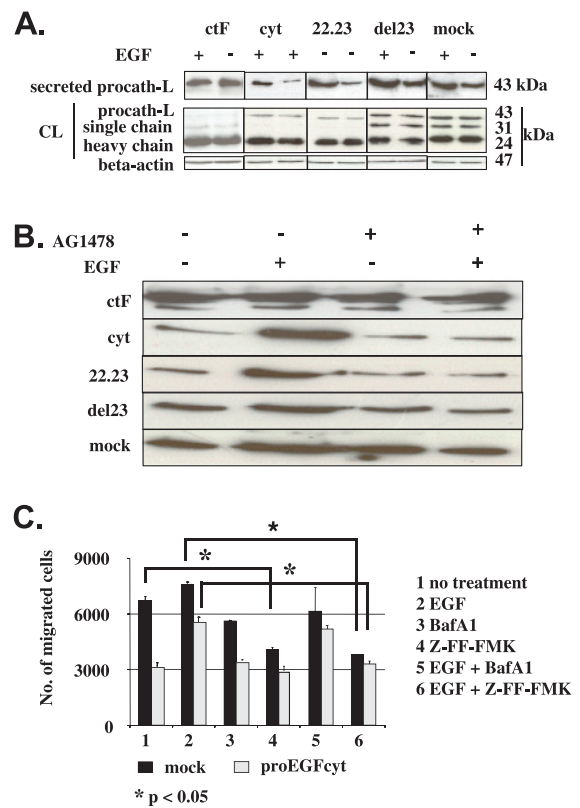
A.

B.

C.

1 no treatment
2 EGF
3 BafA1
4 Z-FF-FMK
5 EGF + BafA1
6 EGF + Z-FF-FMK

■ mock □ proEGFcyt

* p < 0.05

Figure 3. Modulation of elastinolytic activity by proEGFcyt involves regulation of procathepsin L secretion. Western blot detection of the proform (43 kDa), single chain (31 kDa), and the heavy chain of the fully matured form (24 kDa) of cath-L in the supernatants and total CLs of FTC-133 (A). Levels for single-chain form of cath-L were significantly reduced in the presence of proEGFctF, proEGFcyt, and proEGF22.23 but not with proEGF22.23 or in mock controls. Treatment with exogenous EGF caused a significant increase in procath-L secretion particularly in proEGFcyt and proEGF22.23. No increase in secreted procath-L was detected with proEGFctF (A). Protein concentrations in cell lysates and supernatants were determined using both β-actin as a loading control in Western blots and Bradford assay for determining the protein concentration in supernatants, respectively. In contrast to clones expressing the membrane-anchored proEGFctF, FTC-133–proEGFcyt and –proEGF22.23 transfectants showed increased secretion of procath-L on EGF treatment. Involvement of the EGFR was confirmed by the specific EGFR inhibitor AG1478, which abolished the EGF-induced and EGFR-mediated increase in procath-L secretion (B). Representative Western blots of three independent experiments are shown. Elastin migration assays were used to assess the role of lysosomes and cath-L in the elastinolytic migratory phenotype of the transfectants. Cells were treated with exogenous EGF in the presence and absence of the vacuolar H^+–ATPase inhibitor Baf-A1, which prevents acidification of endosomes/lysosomes and the cath-L inhibitor Z-FF-FMK, respectively (C). The ability of clones to penetrate elastin matrices was not affected by Baf-A1 alone or in the presence of exogenous EGF suggesting that the acidic vesicular compartment did not affect the EGF-mediated enhanced elastinolytic migratory activity. In mock transfectants that secrete procath-L, the cath-L inhibitor Z-FF-FMK significantly reduced the ability to penetrate elastin matrices. Z-FF-FMK had no effect on the elastinolytic activity of proEGFcyt transfectants as these cells only secreted very small amounts of detectable procath-L unless stimulated with EGF. Z-FF-FMK abolished the EGF-induced and EGFR-mediated enhanced elastinolytic migration in both proEGFcyt and control transfectants (C) indicating that the elastinolytic migratory activity measured was the result of cath-L–mediated elastin degradation.

Treatment with exogenous EGF did not affect the intracellular processing of cath-L (Figure 3A). With the exception of FTC-133–proEGFctF, EGF caused a marked up-regulation in secreted procath-L in the other FTC-133 transfectants and UTC-8305–proEGFcyt (Figure W1C) and FTC-236 (Figure W2C) transient transfectants. The EGF-induced increase in procath-L secretion was mediated by the EGFR and was abolished in the presence of the EGFR inhibitor AG1478 (Figure 3B). Similar results were obtained with UTC-8305 (Figure W1D) and FTC-236 (Figure W2D). To determine a direct involvement of lysosomes and cath-L in the elastinolytic phenotype, we used the vacuolar H^+–ATPase inhibitor bafilomycin A1 (Baf-A1) that inhibits acidification of endosomes, lysosomes, and phagosomes and the cath-L inhibitor Z-FF-FMK, respectively. Whereas Baf-A1 had no effect, Z-FF-FMK abolished the EGF-induced and EGFR-mediated enhanced elastinolytic migration in the presence of proEGFcyt and mock transfectants (Figure 3C). Similar results were obtained with the FTC-133–proEGFctF transfectants (data not shown). Immunofluorescent analysis of proEGFdel23 and mock cells revealed a focal perinuclear localization of the Golgi and acidic endosome compartments as determined by Golgin-97 (TGN; Figure 4A), M6PR (Figure 4D), and a marked granular peripheral cytoplasmic distribution for lysosomes detected by CD63/LAMP3 (Figure 4G). By contrast, FTC-133–proEGFcyt (Figure 4, B, E, and H) or –proEGF22.23 (data not shown) and FTC-133–proEGFctF transfectants (Figure 4, C, F, and I) showed a circular perinuclear distribution of immunoreactive Golgin-97 (Figure 4, B and C), M6PR (Figure 4, E and F), and CD63/LAMP3 (Figure 4, H and I). In proEGFdel23 and mock controls, procath-L showed a more granular staining pattern (Figure 4J), whereas in the presence of proEGFcyt (Figure 4K), proEGF22.23 (not shown), and EGFctF (Figure 4L), immunoreactive procath-L was frequently localized in the perinuclear space. Transport and maturation of cathepsins are realized by the endolysosomal vesicular system, and disturbances in vesicular distribution/trafficking may affect procath-L processing in the presence of EGFctF and proEGFcyt/proEGF22.23. Marked accumulation of vesicular structures within the cytoplasm of FTC-133–proEGFcyt (Figure 4N) and FTC-133–proEGF22.23 cells, but not proEGFdel23 and mock controls (Figure 4M), was apparent by transmission electron microscopy (Figure 4, M and N).

ProEGFcyt Is a Novel Regulator of SNAP25 Expression and Procath-L Secretion

To identify the molecular mechanism by which EGFctF and proEGFcyt decrease procath-L secretion, we determined the expression of members of the t-SNARE complex known to be important in vesicular-membrane fusion. We established EGFctF as a novel transcriptional activator of SNAP25, isoform A (Figure 5A). Again, juxta- and transmembrane parts of the membrane-anchoring region were dispensable for this effect. Full-size cytoplasmic domain or the synthetic proEGF22.23 gene products were sufficient in the specific up-regulation of *SNAP25* gene activity in FTC-133 (Figure 5B). Similar results were obtained on transient transfection of UTC-8305 (Figure W1E) and FTC-236 (Figure W2E). The presence of EGFctF, proEGFcyt, or proEGF22.23 had no effect on the constitutive expression of the genes encoding *SNAP23* and two other important interacting partners of SNAP25, *syntaxin1A* and *synaptobrevin/VAMP2*, respectively (data not shown). Upon 48 hours of incubation with a specific siRNA for human SNAP25, we observed an almost complete and specific down-regulation of SNAP25 mRNA and protein, whereas a scrambled siRNA control construct had no effect (Figure 5B). Next,

we determined the effect of this *SNAP25* knockdown on the production, processing, and secretion of (pro)cath-L. FTC-133–proEGFctF and –proEGFcyt treated with siRNA-*SNAP25* did not show differences in the production and enzymatic processing of procath-L. However, in the presence of proEGFctF and proEGFcyt, *SNAP25*-knockdown caused a marked up-regulation in the secretion of procath-L by 43% (Figure 5C) and enhanced elastinolytic migration by 46% (Figure 5D). Thus, we identified the proEGFcyt domain as a negative regulator of SNAP25-mediated cath-L secretion. This constitutes a novel pathway associated with elastin matrix invasion of human thyroid carcinoma cells.

ProEGFcyt and EGFR Ligand EGF Regulate SNAP25 Bidirectionally Through Distinct Pathways

We determined the effect of exogenous EGF on SNAP25 mRNA and protein production in FTC-133–EGFctF and proEGFcyt transfectants of the thyroid carcinoma cell lines studied (FTC-133, FTC-236,
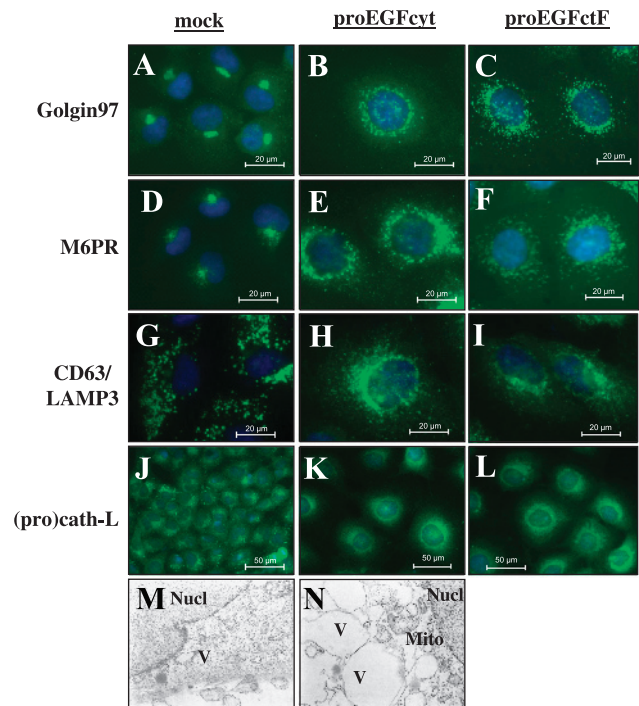

Figure 4. ProEGFcyt and proEGFctF induce altered vesicle and procathepsin L cellular distribution. Immunofluorescent imaging of vesicles of the Golgi-endosomal-lysosomal vesicular compartments in the generally smaller mock cells (A, D, G, J) and the proEGFcyt- (B, E, H, K) and proEGFctF-stable FTC-133 transfectants (C, F, I, L). A significant vesicular phenotype was observed in the presence of proEGFcyt and proEGFctF with altered distribution of TGN (Golgin-97; A–C), acidic endosomes (M6PR; D–F), and lysosomal compartment (CD63/LAMP3; G–I). The proEGFctF, proEGFcyt, and proEGF22.23 clones showed similar results and differed markedly from mock controls that were similar to proEGFdel23 clones (three clones per construct). Distribution of procath-L (J, K, L) in the presence of proEGFcyt (K) and proEGFctF (L) was similar to Golgin-97 (B) and M6PR (E) immunostaining. Mock controls showed a vesicular distribution of procath-L (J) similar to that of lysosomes (G). Representative transmission electron microscopy (TEM) analysis revealed multiple vesicular structures in the cytosol of FTC-133–proEGFcyt transfectants (M). Mock controls did not display this extensive vesicular phenotype (N). *Mito* indicates mitochondria; *V*, vesicles. Original magnifications: A–I, ×620; J–L, ×400; M and N, ×5500.
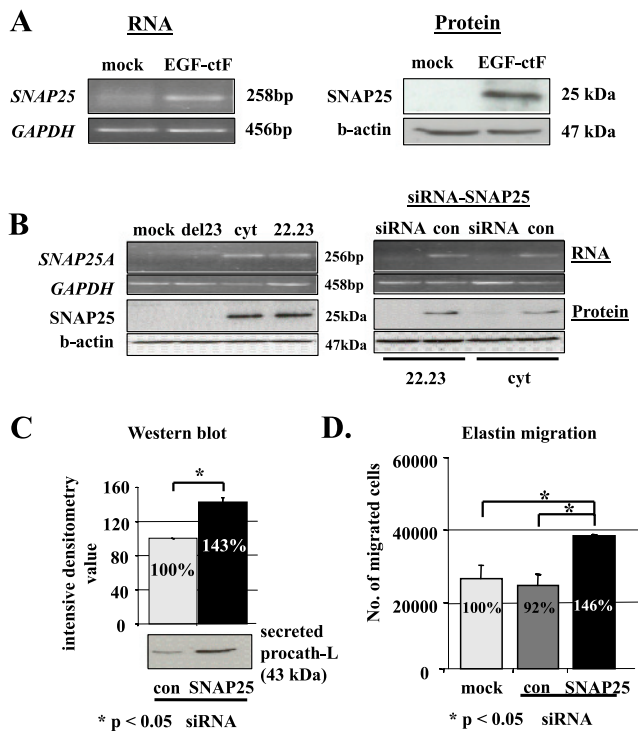
Figure 5. ProEGFctF regulates procathepsin L availability through transcriptional regulation of SNAP25. Using specific primers to human *SNAP25A+B*, RT-PCR analysis revealed a selective up-regulation of *SNAP25A* mRNA expression in the presence of proEGFctF (A). Western blot revealed increased SNAP25 protein production exclusively in proEGFctF transfectants but not in mock controls (A). Similarly, proEGFcyt and proEGF22.23 caused an up-regulation of SNAP25 mRNA and protein (B). A specific siRNA-SNAP25 construct was used to knockdown SNAP25 mRNA expression and protein production (B) in FTC-133–proEGFcyt clones. A nonsilencing, randomized sequence not matching known human genes was used as a control in the siRNA experiments (B). Representative RT-PCR and Western blot analysis of three independent experiments are shown. FTC-133–proEGFcyt and FTC-133–proEGF22.23 transfectants treated with siRNA-SNAP25 or siRNA-control were probed for secreted procath-L using the mAb 2D4 specific for the detection of procath-L. SNAP25 knockdown caused an approximately 43% up-regulation of secreted procath-L when compared to treatment with siRNA-control as shown in a representative Western blot and densitometric analysis (C). This corresponded to a 46% increase in the number of siSNAP15-treated FTC-133–proEGFcyt clones migrating through the elastin matrix (D). Results of three independent experiments with three filter sets per experiments are shown.

and UTC-8305). The decrease in SNAP25 protein observed with EGF treatment was not the result of an EGF-induced down-regulation of *SNAP25* gene activity as determined by RT-PCR (data not shown). Short-term incubations of EGFctF and proEGFcyt clones with EGF for up to 1 hour had no effect on the intracellular SNAP25 protein levels but activated EGFR as determined by the detection of EGFR phosphorylation at residue Tyr 992 in Western blots (data not shown). Treatment with EGF for 4 and 6 hours resulted in a significant down-regulation of SNAP25 protein as shown for proEGFcyt clones (Figure 6, *A* and *B*). This EGF-induced down-regulation of SNAP25 was dependent on the activation of EGFR and was abolished in the presence of AG1478 (Figure 6*A*). When proEGFcyt transfectants of

FTC-133 and UTC-8305 were treated with the two proteasome inhibitors, MG132 or lactacystine, the EGF-induced down-regulation of SNAP25 was abolished indicating that EGF-induced EGFR activation was involved in the proteasomal degradation of SNAP25 as early as 4 hours after EGF exposure in FTC-133–proEGFctF/–proEGFcyt (Figure 6*B*) and UTC-8305–proEGFcyt (Figure W1*E*) and FTC-236 (Figure W2*E*) transient transfectants. Thus, we identified proEGFcyt and the extracellular EGFR ligand EGF to act as functional antagonists
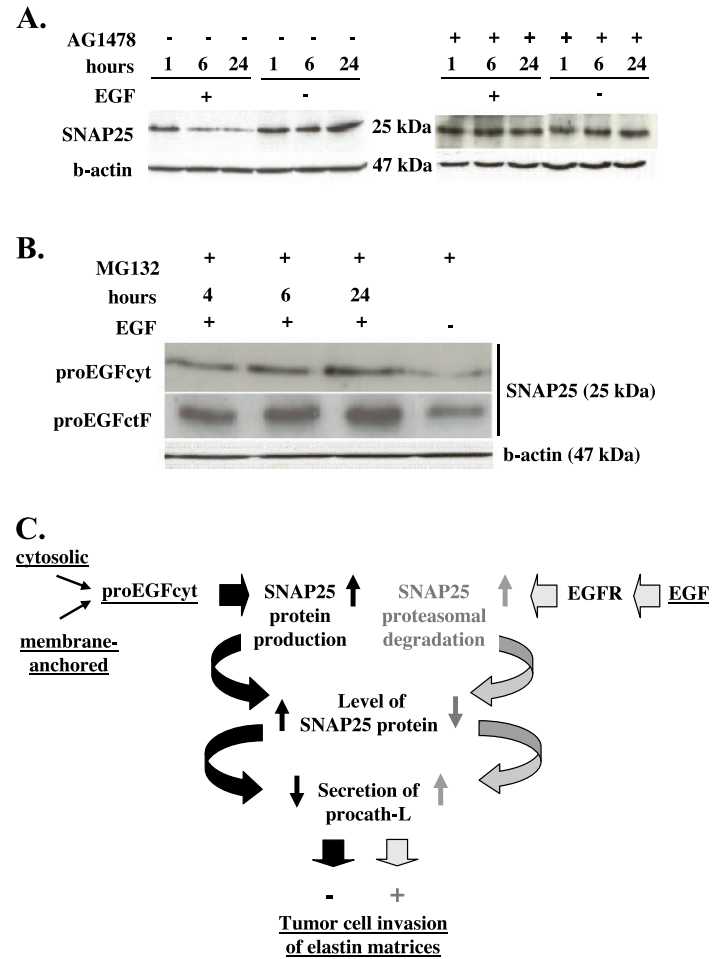

Figure 6. Opposing effects of EGF and proEGFcyt in the presence of SNAP25. Representative Western blots showing SNAP25 protein in FTC-133–proEGFcyt transfectants with and without EGF treatment for 1, 6, and 24 hours in the presence and absence of the specific EGFR inhibitor AG1478 (A). A decrease in SNAP25 immunoreactive protein after 6 hours of incubation with exogenous EGF was observed (A). The EGF-induced decrease in SNAP25 protein production was diminished in the presence of the EGFR inhibitor AG1478 (A). Similar results were obtained with UTC-8305-proEGFcyt and FTC-236-proEGFcyt (Figures W1*E* and W2*E*). Treatment with the proteasomal inhibitor MG132 abolished the EGF-induced down-regulation of SNAP25 protein in FTC-133–proEGFctF and –proEGFcyt clones (B). Beta-actin was used to confirm equal protein loading and representative Western blots of three independent experiments are shown. (C) Schematic illustration of the role of human proEGF (membrane-anchored and cytosolic) and the extracellular EGFR ligand domain, EGF, in affecting elastinolytic invasiveness by human thyroid carcinoma cells. We identified a novel multifaceted role of proEGF functional domains in the regulation of exocytosis and procath-L secretion by human thyroid tumor cells.

by regulating the intracellular level of SNAP25. This affected the secretion of procath-L and the elastinolytic invasion potential of human thyroid carcinoma cells (Figure 6C).

Discussion

The EGF-EGFR ligand-receptor system has important functions in normal thyroid physiology and tumor cell progression/invasiveness and affects the clinical outcome in patients with thyroid carcinoma [35,36]. Using our mouse model of FTC carcinogenesis and a new antiserum specific for proEGFcyt, we detected an inverse relationship between the tissue expression of immunoreactive proEGFcyt, thyroid tumor stage, and enhanced tissue invasion and metastasis. Here, we have investigated the role of the transmembrane region of human proEGF and identified the proEGF cytoplasmic domain as a novel negative regulator of motility and elastinolytic activity in thyroid carcinoma cells. We found that the inhibition of elastinolytic activity and reduced invasion of elastin matrices in the presence of proEGFcyt was caused by the specific transcriptional up-regulation of the t-SNARE component SNAP25 resulting in the reduced secretion of the potent elastinolytic lysosomal hydrolase procath-L. Treatment with EGF antagonized this inhibitory function encoded by proEGFcyt, and both components of human proEGF engaged in different signaling pathways to mediate their opposing cellular actions. The suppressive action of proEGFcyt on thyroid carcinoma cell motility and elastinolytic activity seemed to be independent of EGFR activation, and the peptide sequence encoded by exon 23 was essential for the proEGFcyt-induced cellular actions. We had previously demonstrated a hyperacetylated microtubular phenotype and increased production of the microtubule-associated proteins MAP1b and MAP2c in thyroid carcinoma transfectants expressing proEGFcyt and proEGF22.23 but not a construct with a deletion of exon 23 (proEGFdel23) [27]. The level of tubulin acetylation has been shown to inversely correlate with cell motility [37]. Treatment with exogenous EGF had no effect on the acetylation status of α-tubulin in the proEGFcyt clones tested (T.K., unpublished observations) indicating that this posttranslational microtubular modification was not a likely point of convergence between the enhancing action of EGF and the suppressive effects of proEGFcyt on motility. However, these microtubular changes may have contributed to the unique vesicular distribution detected in proEGFcyt and proEGF22.23 transfectants. In the presence of proEGFctF and proEGFcyt/proEGF22.23, we observed more extensive intracellular processing of the procath-L compared with proEGFdel23 and mock control cells. This likely reflected prolonged exposure of procath-L to the acidic conditions found in late endosomes and lysosomes [38,39]. In the Golgi apparatus, M6P is added specifically to carbohydrates of newly synthesized lysosomal enzymes, and this M6P is used by M6PR located at the inner membrane of the TGN to escort procathepsins from the TGN to the prelysosomal/late endosome acidified compartment [40]. Catalyzed by the acidic pH, the prelysosomal cathepsins dissociate from M6PRs, and final processing of cathepsins takes place in the lysosomes [41]. The acquisition of an elastinolytic phenotype is an important step in the ability of tumor cells to penetrate the basal lamina and initiate the invasion of surrounding tissues [33]. Cath-L has strong elastinolytic activity and is up-regulated in tumor tissues [42,43], including thyroid carcinoma [32,44]. Cath-B, another elastinolytic cathepsin, was not secreted by the thyroid cancer cells studied and, thus, was unlikely to contribute to elastin matrix degradation. Treatment with the cath-L/-B inhibitor Z-FF-FMK [45] abolished the ability of thyroid carcinoma transfectants to pene-

trate elastin matrices indicating that this function was dependent on the secretion of procath-L and cath-L–mediated degradation of elastin. Interestingly, we observed procath-L, but no maturation products thereof, to be the sole cath-L form secreted. Neutralization of the acidic vesicular compartments by the vacuolar H^+–ATPase inhibitor Baf-A1 [46] did not impair the ability of thyroid cancer cells to penetrate elastin matrices. Secretion of procath-L has been observed in normal cells [47,48] and in cells undergoing growth stimulation and malignant transformation [49]. Although procath-L does not seem to have direct elastinolytic activity, extracellular processing of procath-L occurs at the plasma membrane surface at low pH and in the presence of negatively charged surface molecules, e.g., chondroitins or keratan sulfates [50,51]. This is particularly true for tumor cells that acidify their surrounding extracellular milieu [52]. Thus, extracellular (but not intracellular) pH-dependent processing of procath-L likely contributed to the enhanced elastinolytic migratory activity observed in the human follicular and anaplastic thyroid carcinoma transfectants.

ProEGFcyt affected the secretion of procath-L and elastinolytic tumor cell invasiveness by a unique and selective transcriptional up-regulation of SNAP25A in all three thyroid carcinoma cells studied. SNAP25 has previously been implicated as a genetic susceptibility factor for attention-deficient/hyperactivity disorder [53] and dysregulation of insulin secretion from pancreatic β-cells in diabetes [54,55]. The plasma membrane-bound soluble *N*-ethylmaleimide–sensitive factor attachment protein receptor (SNARE) proteins syntaxin1A and synaptosome-associated protein of 25 kDa (SNAP25) and the vesicular SNARE partner vesicle-associated membrane protein (VAMP) are essential components for Ca^{2+}-dependent regulated exocytosis [56,57]. The amino-terminal SNARE motif of SNAP25 engages in a high-affinity heterodimer plasma membrane complex with syntaxin1A and, on interaction with the vesicular synaptobrevin/VAMP, generates the core trimer formation essential for vesicular membrane fusion [58]. Neither proEGFctF nor proEGFcyt affected the expression of ubiquitously present SNAP23, another member of the SNAP25 protein family, suggesting an as yet unknown mechanism by which the proEGF transmembrane region, and here particularly proEGFcyt, can affect *SNAP25* gene activity resulting in changes in exocytosis.

Our data revealed a unique domain-specific involvement of human proEGF in the exocytosis of procath-L–containing vesicles in thyroid cancer cells. By affecting intracellular SNAP25 protein levels in opposite ways, the soluble extracellular EGFR ligand EGF and the intracellular proEGFcyt were identified as novel regulatory factors able to modulate procath-L secretion and elastin invasion in thyroid tumor cells. It has previously been shown that the specific stoichiometry of the anchoring proteins syntaxin1A and SNAP25 is a decisive determinant for efficient vesicle fusion with the plasma membrane and has a direct impact on the exocytotic efficacy and associated biologic functions. Changes in protein levels of either SNAP25 or syntaxin1A were shown to decrease glucose-stimulated insulin release in normal rat islets [54,59], but the regulatory elements of these processes remain largely unknown.

In conclusion, the transcriptional up-regulation of *SNAP25* gene activity by proEGFctF and proEGFcyt and the proteasomal degradation of SNAP25 protein by EGF-induced EGFR activation provide a novel system for tumor cell invasiveness. This may have implications beyond human thyroid carcinoma and reflect a molecular mechanism effective in physiological processes and in other proEGF-producing cancers.

Acknowledgments

References

[1] Bell GI, Fong NM, Stempien MM, Wormsted MA, Caput D, Ku LL, Urdea MS, Rall LB, and Sanchez-Pescador R (1986). Human epidermal growth factor precursor: cDNA sequence, expression *in vitro* and gene organization. *Nucleic Acids Res* **14**, 8427–8446.

[2] Massague J and Pandiella A (1993). Membrane-anchored growth factors. *Annu Rev Biochem* **62**, 515–541.

[3] Normanno N, De Luca A, Bianco C, Strizzi L, Mancino M, Maiello MR, Carotenuto A, De Feo G, Caponigro F, and Salomon DS (2006). Epidermal growth factor receptor (EGFR) signaling in cancer. *Gene* **366**, 2–16.

[4] Dong J, Opresko LK, Chrisler W, Orr G, Quesenberry RD, Lauffenburger DA, and Wiley HS (2005). The membrane-anchoring domain of epidermal growth factor receptor ligands dictates their ability to operate in juxtacrine mode. *Mol Biol Cell* **16**, 2984–2998.

[5] Dong J and Wiley HS (2000). Trafficking and proteolytic release of epidermal growth factor receptor ligands are modulated by their membrane-anchoring domains. *J Biol Chem* **275**, 557–564.

[6] Fisher DA, Salido EC, and Barajas L (1989). Epidermal growth factor and the kidney. *Annu Rev Physiol* **51**, 67–80.

[7] Salido EC, Yen PH, Shapiro LJ, Fisher DA, and Barajas L (1989). *In situ* hybridization of prepro-epidermal growth factor mRNA in the mouse kidney. *Am J Physiol* **256**, F632–F638.

[8] Salido EC, Lakshmanan J, Shapiro LJ, Fisher DA, and Barajas L (1990). Expression of epidermal growth factor in the kidney and submandibular gland during mouse postnatal development. An immunocytochemical and *in situ* hybridization study. *Differentiation* **45**, 38–43.

[9] Dempsey PJ, Meise KS, Yoshitake Y, Nishikawa K, and Coffey RJ (1997). Apical enrichment of human EGF precursor in Madin-Darby canine kidney cells involves preferential basolateral ectodomain cleavage sensitive to a metalloprotease inhibitor. *J Cell Biol* **138**, 747–758.

[10] Shum L, Reeves SA, Kuo AC, Fromer ES, and Derynck R (1994). Association of the transmembrane TGF-alpha precursor with a protein kinase complex. *J Cell Biol* **125**, 903–916.

[11] Fernandez-Larrea J, Merlos-Suarez A, Urena JM, Baselga J, and Arribas J (1999). A role for a PDZ protein in the early secretory pathway for the targeting of proTGF-alpha to the cell surface. *Mol Cell* **3**, 423–433.

[12] Kuo A, Zhong C, Lane WS, and Derynck R (2000). Transmembrane transforming growth factor-alpha tethers to the PDZ domain-containing, Golgi membrane–associated protein p59/GRASP55. *EMBO J* **19**, 6427–6439.

[13] Franklin JL, Yoshiura K, Dempsey PJ, Bogatcheva G, Jeyakumar L, Meise KS, Pearsall RS, Threadgill D, and Coffey RJ (2005). Identification of MAGI-3 as a transforming growth factor-alpha tail binding protein. *Exp Cell Res* **303**, 457–470.

[14] Li C, Franklin JL, Graves-Deal R, Jerome WG, Cao Z, and Coffey RJ (2004). Myristoylated Naked2 escorts transforming growth factor alpha to the basolateral plasma membrane of polarized epithelial cells. *Proc Natl Acad Sci USA* **101**, 5571–5576.

[15] Dempsey PJ and Coffey RJ (1994). Basolateral targeting and efficient consumption of transforming growth factor-alpha when expressed in Madin-Darby canine kidney cells. *J Biol Chem* **269**, 16878–16889.

[16] Dempsey PJ, Meise KS, and Coffey RJ (2003). Basolateral sorting of transforming growth factor-alpha precursor in polarized epithelial cells: characterization of cytoplasmic domain determinants. *Exp Cell Res* **285**, 159–174.

[17] Brown CL, Coffey RJ, and Dempsey PJ (2001). The proamphiregulin cytoplasmic domain is required for basolateral sorting, but is not essential for constitutive or stimulus-induced processing in polarized Madin-Darby canine kidney cells. *J Biol Chem* **276**, 29538–29549.

[18] Adam RM, Danciu T, McLellan DL, Borer JG, Lin J, Zurakowski D, Weinstein MH, Rajjayabun PH, Mellon JK, and Freeman MR (2003). A nuclear form of the heparin-binding epidermal growth factor-like growth factor precursor is a feature of aggressive transitional cell carcinoma. *Cancer Res* **63**, 484–490.

[19] Lin J, Hutchinson L, Gaston SM, Raab G, and Freeman MR (2001). BAG-1 is a novel cytoplasmic binding partner of the membrane form of heparin-binding EGF-like growth factor: a unique role for proHB-EGF in cell survival regulation. *J Biol Chem* **276**, 30127–30132.

[20] Hieda M, Isokane M, Koizumi M, Higashi C, Tachibana T, Shudou M, Taguchi T, Hieda Y, and Higashiyama S (2008). Membrane-anchored growth factor, HB-EGF, on the cell surface targeted to the inner nuclear membrane. *J Cell Biol* **180**, 763–769.

[21] Kinugasa Y, Hieda M, Hori M, and Higashiyama S (2007). The carboxyl-terminal fragment of pro–HB-EGF reverses *Bcl6*-mediated gene repression. *J Biol Chem* **282**, 14797–14806.

[22] Nanba D and Higashiyama S (2004). Dual intracellular signaling by proteolytic cleavage of membrane-anchored heparin-binding EGF-like growth factor. *Cytokine Growth Factor Rev* **15**, 13–19.

[23] Wang X, Mizushima H, Adachi S, Ohishi M, Iwamoto R, and Mekada E (2006). Cytoplasmic domain phosphorylation of heparin-binding EGF-like growth factor. *Cell Struct Funct* **31**, 15–27.

[24] Bao J, Wolpowitz D, Role LW, and Talmage DA (2003). Back signaling by the Nrg-1 intracellular domain. *J Cell Biol* **161**, 1133–1141.

[25] Wang JY, Frenzel KE, Wen D, and Falls DL (1998). Transmembrane neuregulins interact with LIM kinase 1, a cytoplasmic protein kinase implicated in development of visuospatial cognition. *J Biol Chem* **273**, 20525–20534.

[26] Bao J, Lin H, Ouyang Y, Lei D, Osman A, Kim TW, Mei L, Dai P, Ohlemiller KK, and Ambron RT (2004). Activity-dependent transcription regulation of PSD-95 by neuregulin-1 and Eos. *Nat Neurosci* **7**, 1250–1258.

[27] Pyka J, Glogowska A, Dralle H, Hoang-Vu C, and Klonisch T (2005). Cytoplasmic domain of proEGF affects distribution and post-translational modification of microtubuli and increases microtubule-associated proteins 1b and 2 production in human thyroid carcinoma cells. *Cancer Res* **65**, 1343–1351.

[28] Suzuki H, Willingham MC, and Cheng SY (2002). Mice with a mutation in the thyroid hormone receptor beta gene spontaneously develop thyroid carcinoma: a mouse model of thyroid carcinogenesis. *Thyroid* **12**, 963–969.

[29] Ying H, Suzuki H, Zhao L, Willingham MC, Meltzer P, and Cheng SY (2003). Mutant thyroid hormone receptor beta represses the expression and transcriptional activity of peroxisome proliferator–activated receptor gamma during thyroid carcinogenesis. *Cancer Res* **63**, 5274–5280.

[30] Kato Y, Ying H, Willingham MC, and Cheng SY (2004). A tumor suppressor role for thyroid hormone beta receptor in a mouse model of thyroid carcinogenesis. *Endocrinology* **145**, 4430–4438.

[31] Tolosa E, Li W, Yasuda Y, Wienhold W, Denzin LK, Lautwein A, Driessen C, Schnorrer P, Weber E, Stevanovic S, et al. (2003). Cathepsin V is involved in the degradation of invariant chain in human thymus and is overexpressed in *Myasthenia gravis*. *J Clin Invest* **112**, 517–526.

[32] Hombach-Klonisch S, Bialek J, Trojanowicz B, Weber E, Holzhausen HJ, Silvertown JD, Summerlee AJ, Dralle H, Hoang-Vu C, and Klonisch T (2006). Relaxin enhances the oncogenic potential of human thyroid carcinoma cells. *Am J Pathol* **169**, 617–632.

[33] Hornebeck W and Maquart FX (2003). Proteolyzed matrix as a template for the regulation of tumor progression. *Biomed Pharmacother* **57**, 223–230.

[34] Timar J, Diczhazi C, Ladanyi A, Raso E, Hornebeck W, Robert L, and Lapis K (1995). Interaction of tumour cells with elastin and the metastatic phenotype. *Ciba Found Symp* **192**, 321–335discussion 335–337.

[35] Hoelting T, Siperstein AE, Clark OH, and Duh QY (1994). Epidermal growth factor enhances proliferation, migration, and invasion of follicular and papillary thyroid cancer *in vitro* and *in vivo*. *J Clin Endocrinol Metab* **79**, 401–408.

[36] Younes MN, Yigitbasi OG, Park YW, Kim SJ, Jasser SA, Hawthorne VS, Yazici YD, Mandal M, Bekele BN, Bucana CD, et al. (2005). Antivascular therapy of human follicular thyroid cancer experimental bone metastasis by blockade of epidermal growth factor receptor and vascular growth factor receptor phosphorylation. *Cancer Res* **65**, 4716–4727.

[37] Palazzo A, Ackerman B, and Gundersen GG (2003). Cell biology: tubulin acetylation and cell motility. *Nature* **421**, 230.

[38] Nomura T and Fujisawa Y (1997). Processing properties of recombinant human procathepsin L. *Biochem Biophys Res Commun* **230**, 143–146.

[39] Ishidoh K and Kominami E (2002). Processing and activation of lysosomal proteinases. *Biol Chem* **383**, 1827–1831.

[40] von Figura K and Hasilik A (1986). Lysosomal enzymes and their receptors. *Annu Rev Biochem* **55**, 167–193.

[41] Le Borgne R and Hoflack B (1998). Protein transport from the secretory to the endocytic pathway in mammalian cells. *Biochim Biophys Acta* **1404**, 195–209.

[42] Fehrenbacher N and Jaattela M (2005). Lysosomes as targets for cancer therapy. *Cancer Res* **65**, 2993–2995.

[43] Krueger S, Kellner U, Buehling F, and Roessner A (2001). Cathepsin L antisense oligonucleotides in a human osteosarcoma cell line: effects on the invasive phenotype. *Cancer Gene Ther* **8**, 522–528.

[44] Friedrichs B, Tepel C, Reinheckel T, Deussing J, von Figura K, Herzog V, Peters C, Saftig P, and Brix K (2003). Thyroid functions of mouse cathepsins B, K, and L. *J Clin Invest* **111**, 1733–1745.

[45] Ravanko K, Jarvinen K, Helin J, Kalkkinen N, and Holtta E (2004). Cysteine cathepsins are central contributors of invasion by cultured adenosylmethionine decarboxylase–transformed rodent fibroblasts. *Cancer Res* **64**, 8831–8838.

[46] Yoshimori T, Yamamoto A, Moriyama Y, Futai M, and Tashiro Y (1991). Bafilomycin A1, a specific inhibitor of vacuolar-type H(+)–ATPase, inhibits acidification and protein degradation in lysosomes of cultured cells. *J Biol Chem* **266**, 17707–17712.

[47] Reilly JJ Jr, Mason RW, Chen P, Joseph LJ, Sukhatme VP, Yee R, and Chapman HA Jr (1989). Synthesis and processing of cathepsin L, an elastase, by human alveolar macrophages. *Biochem J* **257**, 493–498.

[48] Hamilton RT, Bruns KA, Delgado MA, Shim JK, Fang Y, Denhardt DT, and Nilsen-Hamilton M (1991). Developmental expression of cathepsin L and c-rasHa in the mouse placenta. *Mol Reprod Dev* **30**, 285–292.

[49] Achkar C, Gong QM, Frankfater A, and Bajkowski AS (1990). Differences in targeting and secretion of cathepsins B and L by BALB/3T3 fibroblasts and Moloney murine sarcoma virus–transformed BALB/3T3 fibroblasts. *J Biol Chem* **265**, 13650–13654.

[50] Reddy VY, Zhang QY, and Weiss SJ (1995). Pericellular mobilization of the tissue-destructive cysteine proteinases, cathepsins B, L, and S, by human monocyte–derived macrophages. *Proc Natl Acad Sci USA* **92**, 3849–3853.

[51] Mason RW and Massey SD (1992). Surface activation of pro-cathepsin L. *Biochem Biophys Res Commun* **189**, 1659–1666.

[52] Montcourrier P, Silver I, Farnoud R, Bird I, and Rochefort H (1997). Breast cancer cells have a high capacity to acidify extracellular milieu by a dual mechanism. *Clin Exp Metastasis* **15**, 382–392.

[53] Feng Y, Crosbie J, Wigg K, Pathare T, Ickowicz A, Schachar R, Tannock R, Roberts W, Malone M, Swanson J, et al. (2005). The *SNAP25* gene as a susceptibility gene contributing to attention-deficit hyperactivity disorder. *Mol Psychiatry* **10**, 998–1005973.

[54] Nagamatsu S, Nakamichi Y, Yamamura C, Matsushima S, Watanabe T, Ozawa S, Furukawa H, and Ishida H (1999). Decreased expression of t-SNARE, syntaxin 1, and SNAP-25 in pancreatic beta-cells is involved in impaired insulin secretion from diabetic GK rat islets: restoration of decreased t-SNARE proteins improves impaired insulin secretion. *Diabetes* **48**, 2367–2373.

[55] Gonelle-Gispert C, Halban PA, Niemann H, Palmer M, Catsicas S, and Sadoul K (1999). SNAP-25a and -25b isoforms are both expressed in insulin-secreting cells and can function in insulin secretion. *Biochem J* **339** (Pt 1), 159–165.

[56] Sudhof TC (1995). The synaptic vesicle cycle: a cascade of protein-protein interactions. *Nature* **375**, 645–653.

[57] Salaun C, James DJ, Greaves J, and Chamberlain LH (2004). Plasma membrane targeting of exocytic SNARE proteins. *Biochim Biophys Acta* **1693**, 81–89.

[58] McMahon HT and Sudhof TC (1995). Synaptic core complex of synaptobrevin, syntaxin, and SNAP25 forms high affinity alpha-SNAP binding site. *J Biol Chem* **270**, 2213–2217.

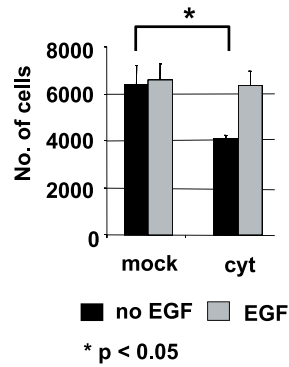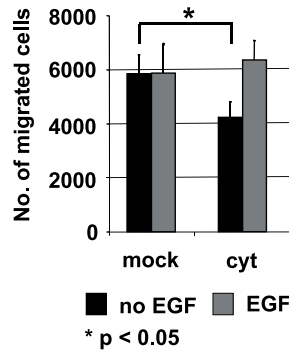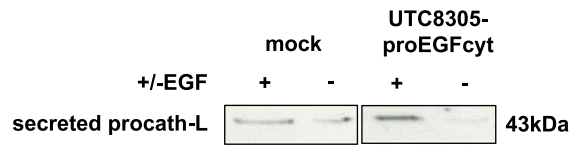[59] Weimbs T, Low SH, Li X, and Kreitzer G (2003). SNAREs and epithelial cells. *Methods* **30**, 191–197.
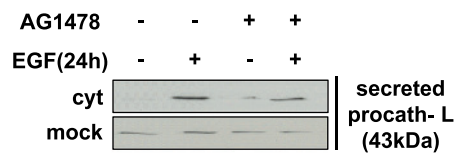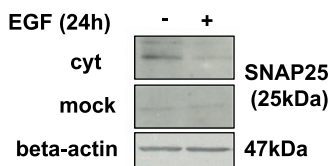
Figure W1. (A) Reduced motility of UTC-8305 transiently transfected with the human proEGFcyt construct. Exogenous EGF antagonized this motility-suppressive effect of proEGFcyt. (B) Transient expression of proEGFcyt impaired the ability of UTC-8305 to migrate through the elastin matrix, and this inhibitory effect was counteracted by soluble EGF. (C) UTC-8305 displayed significantly decreased secretion of procath-L in the presence of proEGFcyt. Incubation with soluble EGF reversed this phenotype and resulted in markedly enhanced secretion of procath-L. Epidermal growth factor treatment had no effect on untransfected or mock-treated UTC-8305. (D) The increase in the secretion of procath-L by soluble EGF was mediated by the EGFR and was inhibited in the presence of the specific EGFR inhibitor AG1478. No change in procath-L secretion was observed in mock controls on treatment with soluble EGF, AG1478, or DMSO solvent (data not shown). (E) In the presence of transiently expressed proEGFcyt, UTC-8305 displayed an up-regulation of *SNAP25* mRNA (not shown) and SNAP25 protein (25 kDa). Treatment with exogenous EGF resulted in a significant decrease in SNAP25 production. Equal protein loading was confirmed with β-actin. All Western blots are representative examples of three independent experiments.
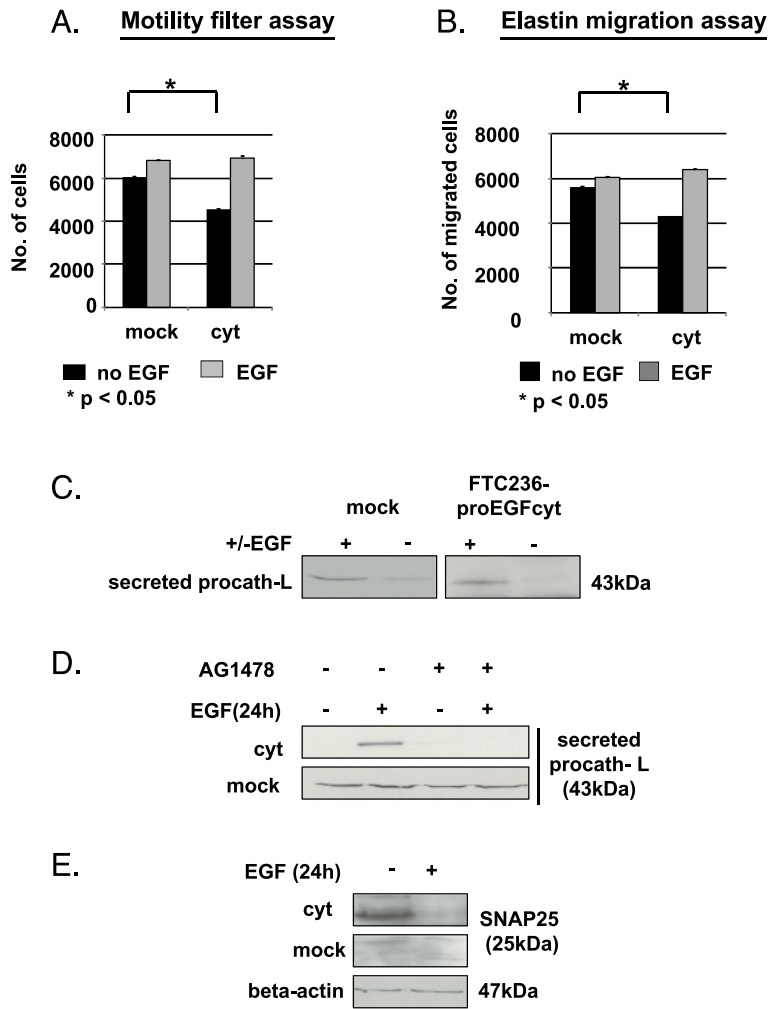
Figure W2. (A) Transient transfection of FTC-236 cells using proEGFcyt construct resulted in a decrease in tumor cell motility. Treatment with soluble EGF antagonized the inhibitory action of proEGFcyt and significantly increased motility of FTC-236. (B) Similar inhibitory action of proEGFcyt was observed during cell migration through an elastin matrix and exogenous EGF enhanced elastinolytic migratory activity. (C) ProEGFcyt inhibited secretion of procath-L in FTC-236, and this effect was counteracted by soluble EGF. (D) The increase in the secretion of procath-L by soluble EGF was mediated by the EGFR and inhibited in the presence of AG1478. (E) In the presence of proEGFcyt, both mRNA and protein level of SNAP 25 were up-regulated in FTC-236 and treatment with soluble EGF decreases protein level of SNAP25.
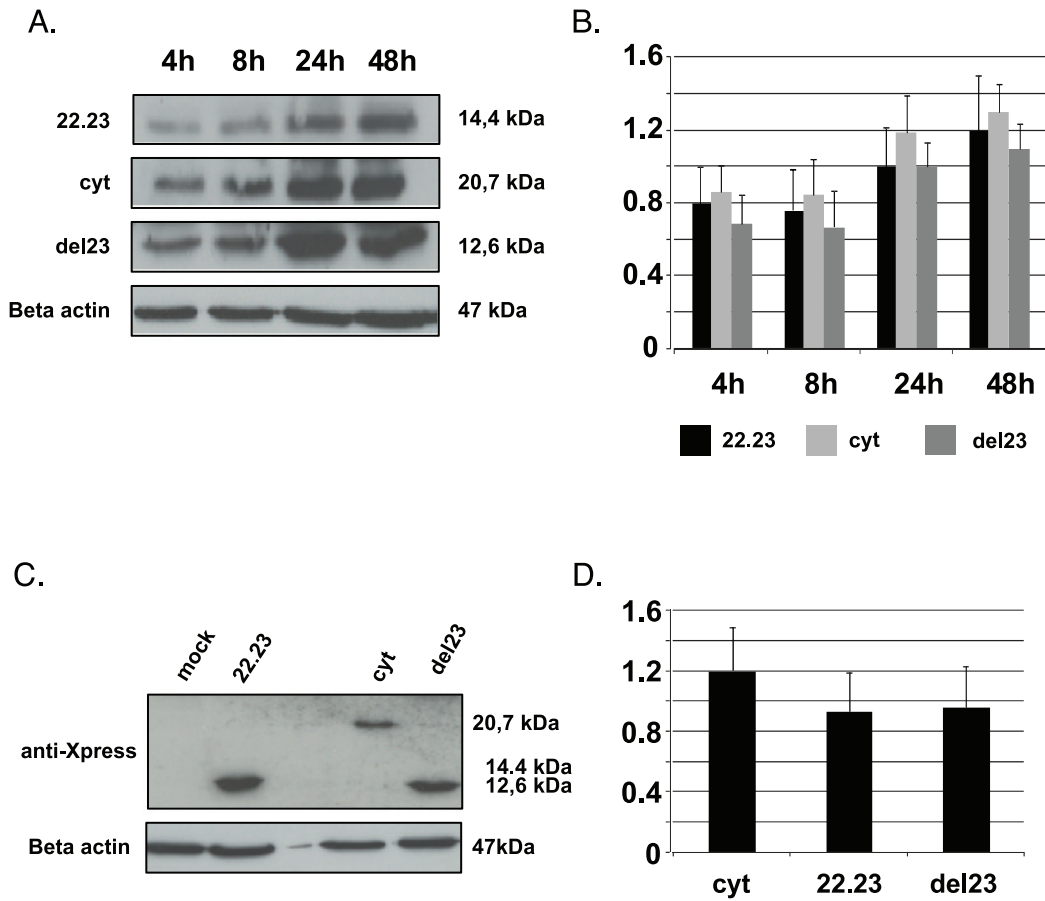
Figure W3. (A) Western blot detection of proEGFcyt using the rabbit polyclonal antiserum against human proEGFcyt. ProEGFcyt protein content was monitored at 4, 8, 24, and 48 hours of culture. Higher protein concentrations of proEGFcyt detected at 24 and 48 hours coincided with higher numbers of cells per well at these time points as verified by β-actin and (B) corresponding densitometry representing three independent experiments. (C) Detection of proEGFcyt using the anti-Xpress tag antibody. (D) Again, densitometry of six independent Western blot analyses failed to show significant difference in protein content for the different proEGF mutant proteins at 24 hours in FTC-133 transfectants. β-Actin was used to determine the relative amount of proteins for densitometric measurements. In conclusion, different stable transfectants contained similar amounts of proEGF recombinant proteins over time. The same protein extracts had been used for the detection of SNAP25 and procath-L.